

ACCEPTED MANUSCRIPT • OPEN ACCESS

## Stabilization of an iridium oxygen evolution catalyst by titanium oxides

To cite this article before publication: Olga Kasian *et al* 2020 *J. Phys. Energy* in press <https://doi.org/10.1088/2515-7655/abbd34>

### Manuscript version: Accepted Manuscript

Accepted Manuscript is “the version of the article accepted for publication including all changes made as a result of the peer review process, and which may also include the addition to the article by IOP Publishing of a header, an article ID, a cover sheet and/or an ‘Accepted Manuscript’ watermark, but excluding any other editing, typesetting or other changes made by IOP Publishing and/or its licensors”

This Accepted Manuscript is © 2020 The Author(s). Published by IOP Publishing Ltd.

As the Version of Record of this article is going to be / has been published on a gold open access basis under a CC BY 3.0 licence, this Accepted Manuscript is available for reuse under a CC BY 3.0 licence immediately.

Everyone is permitted to use all or part of the original content in this article, provided that they adhere to all the terms of the licence <https://creativecommons.org/licenses/by/3.0>

Although reasonable endeavours have been taken to obtain all necessary permissions from third parties to include their copyrighted content within this article, their full citation and copyright line may not be present in this Accepted Manuscript version. Before using any content from this article, please refer to the Version of Record on IOPscience once published for full citation and copyright details, as permissions may be required. All third party content is fully copyright protected and is not published on a gold open access basis under a CC BY licence, unless that is specifically stated in the figure caption in the Version of Record.

View the [article online](#) for updates and enhancements.

## Stabilization of an Iridium Oxygen Evolution Catalyst by Titanium Oxides

Olga Kasian<sup>1,2,3,\*</sup>, Tong Li<sup>4</sup>, Andrea M. Mingers<sup>2</sup>, Kevin Schweinar<sup>2</sup>, Alan Savan<sup>5</sup>, Alfred Ludwig<sup>5</sup>, Karl Mayrhofer<sup>6,7</sup>

<sup>1</sup> Helmholtz-Zentrum Berlin GmbH, Helmholtz Institut Erlangen-Nürnberg, Hahn-Meitner-Platz 1, 14109 Berlin, Germany, e-mail: [olga.kasian@helmholtz-berlin.de](mailto:olga.kasian@helmholtz-berlin.de)

<sup>2</sup> Max-Planck-Institut für Eisenforschung GmbH, Max-Planck-Str. 1, 40237 Düsseldorf, Germany

<sup>3</sup> Department of Materials Science and Engineering, Friedrich-Alexander-Universität Erlangen-Nürnberg, 91058 Erlangen, Germany

<sup>4</sup> Institute for Materials & Zentrum für Grenzflächendominierte Höchstleistungswerkstoffe (ZGH), Ruhr-Universität Bochum, 44801 Bochum, Germany

<sup>5</sup> Chair for Materials Discovery and Interfaces, Institute for Materials, Faculty of Mechanical Engineering, Ruhr-Universität Bochum, 44801 Bochum, Germany

<sup>6</sup> Helmholtz-Institute Erlangen-Nürnberg for Renewable Energy (IEK-11), Forschungszentrum Jülich GmbH, 91058 Erlangen, Germany

<sup>7</sup> Department of Chemical and Biological Engineering, Friedrich-Alexander-Universität Erlangen-Nürnberg, 91058 Erlangen, Germany

### Abstract

The anodic oxygen evolution reaction has significant importance in many electrochemical technologies. In proton exchange membrane water electrolyzers it plays a pivotal role for electrochemical energy conversion, yet sluggish kinetics and the corrosive environment during operation still compel significant advances in electrode materials to enable a widespread application. Up to date Iridium is known as the best catalyst material for the oxygen evolution reaction in acidic media due to its relatively high activity and long-term stability. However, scarcity of iridium drives the development of strategies for its efficient utilization. One of the promising ways would be the formation of mixtures in which the noble catalyst element is dispersed in the non-noble matrix of more stable metals or metal oxides. A promising valve metal oxide is  $\text{TiO}_x$ , yet the degree to which performance can be optimized by composition is still unresolved. Thus, using a scanning flow cell connected to an inductively coupled plasma mass spectrometer, we examined the activity and stability for the oxygen evolution reaction of an oxidized Ir-Ti thin film material library covering the composition range from 20 – 70 at.% of Ir. We find that regardless of the composition the rate of Ir dissolution is observed to be lower than that of thermally prepared  $\text{IrO}_2$ . Moreover, mixtures containing at least 50 at.% of Ir exhibit reactivity comparable to  $\text{IrO}_2$ . Their superior performance is discussed with complementary information obtained from atomic scale and electronic structure analysis using atom probe tomography and X-ray photoelectron spectroscopy. Overall, our data show that Ir-Ti mixtures can be promising OER catalysts with both high activity and high stability.

### Introduction

1  
2  
3 With increasing environmental concerns, sustainable energy sources are anticipated to eventually replace  
4 traditional fossil fuels. However, such transition demands development of environmentally friendly  
5 solutions for energy conversion and storage, especially due to the intermittent nature of renewables. In  
6 this regard, the balance between power generated by renewables and energy demand for end-use can be  
7 achieved by using electrochemical water splitting to produce hydrogen as the energy storage medium [1-  
8 3]. Proton exchange membrane water electrolysis (PEMWE) is considered as one of the most promising  
9 technologies for this purpose [4]. However, the widespread application of PEMWE is limited mainly by  
10 high cost and low efficiency of the electrocatalyst materials [5]. Materials that catalyze water  
11 decomposition should provide high reactivity and maintain stability throughout long-time operation. This  
12 is especially crucial in case of the anodic oxygen evolution reaction (OER), due to the extremely corrosive  
13 acidic environment and the high potential required to drive this reaction [6-8]. Only a few materials are  
14 able to meet the necessary requirements to simultaneously provide sufficient reactivity and durability in  
15 harsh oxidizing conditions [9, 10]. Typically those are oxides with metallic-type conductivity, among which  
16 only iridium oxides are currently used in acidic water electrolyzers [4, 11, 12]. Nevertheless, even Ir-based  
17 catalysts slowly undergo dissolution [13-17]. Considering the scarcity and high price of Ir, optimization of  
18 its utilization and suppression of degradation become of pivotal importance. Mixing of Ir with other more  
19 stable materials, e.g. Ti [18-22] or Sn [23-25] typically results in catalysts showing very high stability against  
20 dissolution, but leads to penalties in terms of reactivity. Electrocatalytic performance deteriorates  
21 because of the inactivity of the non-noble surface elements and the insulating nature of stoichiometric  
22  $\text{TiO}_2$  and  $\text{SnO}_2$  [19-21]. Nevertheless, the idea of mixing Ti and Ir in an optimized ratio remains attractive  
23 for achieving a beneficial compromise between catalytic activity and stability at low noble metal loading.  
24 During the last decades, numerous research efforts have been focused on the electrochemical and surface  
25 properties of anodes based on such alloys or oxides, and the current utilization of  $\text{TiO}_2$  [26-28] and  $\text{SnO}_2$   
26 [29, 30] as catalyst supports for Ir catalyst nanoparticles confirms the success of the approach. Particularly,  
27 Ir-Ti oxide systems can maintain good reactivity during long term operation [21, 31, 32], yet a systematic  
28 investigation of the dependence of the performance on Ir-Ti composition with identical morphologies and  
29 operation conditions is still missing. Moreover, the origin of the improved stability in such systems and  
30 the interplay between composition and activity-stability trends remains an open question.  
31  
32  
33  
34  
35  
36  
37  
38  
39

40 Herein, OER reactivity and stability of model Ir- $\text{TiO}_x$  thin film electrodes covering a wide composition range  
41 are evaluated in acidic media using an electrochemical scanning flow cell connected to an inductively  
42 coupled plasma mass spectrometer (SFC-ICP-MS). Identical experimental protocols are applied in order to  
43 obtain systematic and comparable information on electrocatalytic properties of these catalysts. It is found  
44 that materials containing 40 – 50 at.% of Ir exhibit reactivity comparable to thermally prepared  $\text{IrO}_2$ , with  
45 dissolution below the detection limit of the ICP-MS. The obtained results on activity and stability trends  
46 for the Ir- $\text{TiO}_x$  electrodes are compared to Ir-Ru and Ir-Sn mixed oxides and discussed in light of their  
47 potential utilization in water electrolyzers.  
48  
49  
50  
51  
52

## 53 Experimental

54  
55  
56  
57  
58  
59  
60

1  
2  
3 The details on experimental setups and Ir-Ti thin-film material library characterization are shown in the  
4 Supplementary information (SI, Fig. S1 - S3). In short, the material libraries of Ir-Ti alloys were prepared  
5 by combinatorial-magnetron sputtering (DCA Instruments, Turku, Finland) employing a con-focal co-  
6 deposition approach (Fig. S1). Single crystal Si wafers (100) with a 1.5  $\mu\text{m}$  barrier layer of thermal  $\text{SiO}_2$   
7 were used as substrates. Using such smooth substrates allows preparation of samples with minimized  
8 surface roughness. The substrates were cleaned in acetone and then isopropanol in an ultrasonic bath  
9 and dried with compressed, dry air before loading to the deposition chamber. The base pressure in the  
10 main chamber prior to deposition did not exceed  $2.7 \cdot 10^{-6}$  Pa. The 100 mm diameter targets of Ti  
11 (99.995%, FHR, Germany) and Ir (99.9%, Evochem, Germany) were precleaned by sputtering with closed  
12 shutters prior to deposition. Ar (99.999%) was used as the sputter gas and the pressure in the chamber  
13 was adjusted to 0.67 Pa at room temperature. A 20 nm Ti adhesion layer was deposited at 200 W RF with  
14 a constant substrate rotation of 20 rpm, in order to produce uniform layer thicknesses from the confocal  
15 cathode arrangement. Then Ir and Ti were deposited simultaneously at 79 W RF and 157 W RF,  
16 respectively. The total growth rate was  $0.03 \text{ nm s}^{-1}$ . Due to the confocal cathode arrangement and the  
17 cathode tilt with respect to the substrate surface, thickness gradients are produced (see Fig. S4) when the  
18 substrate is static. As a result, the composition ratio of the co-sputtered elements in the mixture is  
19 dependent on the position on the sample surface. The composition of the obtained libraries was  
20 confirmed using EDX mapping as shown in Fig. S3 (INCA X-act, Oxford Instruments, U.K.) and X-ray  
21 photoelectron spectroscopy (XPS). After deposition, the samples were thermally treated in air at  $350 \text{ }^\circ\text{C}$   
22 for 4 h. This procedure leads to the formation of a continuous composition spread of oxide films with  
23 different Ti and Ir contents. After the high-throughput characterization of the material library for desired  
24 properties, the most promising compositions were synthesized as individual samples.

25  
26 XPS measurements were performed to ensure the composition of the material library after annealing  
27 (Quantera II, Physical Electronics, Chanhassen, MN, USA). A monochromatic Al K $\alpha$ X-ray source (1486.6  
28 eV) was applied at 15 kV and 25 W. The binding energy scale was referenced to the C 1s signal at 285.0  
29 eV. Analysis of the spectra was carried out using the Casa XPS (<http://www.casaxps.com/>) software. The  
30 compositions of the electrodes are shown in Ir–Ti atomic ratios, omitting oxygen. The Ir–Ti oxide library  
31 was then used as the working electrode in the scanning flow cell (SFC) – inductively coupled plasma mass  
32 spectrometer (ICP-MS, NexION 350X, Perkin Elmer) based setup [33, 34]. The geometric surface area of  
33 the working electrode was defined by the size of the opening of the SFC (ca.  $1 \cdot 10^{-2} \text{ cm}^2$ ). All presented  
34 data are normalized to the geometric area of the working electrode. The inlet channel of the SFC  
35 contained a graphite rod, serving as the counter electrode. A commercial Ag/AgCl/3M KCl electrode  
36 (Metrohm, Germany) was used as the reference electrode. The reversible hydrogen electrode (RHE)  
37 potential was measured in  $\text{H}_2$ -saturated electrolyte using a freshly prepared sputtered Pt thin film versus  
38 the saturated Ag/AgCl electrode. All potentials reported in the manuscript are presented versus the RHE  
39 scale. All electrochemical measurements were carried out in 0.1 M  $\text{HClO}_4$  solution prepared by dilution of  
40 concentrated perchloric acid (Suprapur 96%, Merck, Germany) in ultrapure water (PureLabPlus system,  
41 Elga, 18 M $\Omega$ cm, TOC<3 ppb). During measurements, the argon-saturated electrolyte was pumped with a  
42 constant flow rate of ca.  $196 \mu\text{Lmin}^{-1}$  to the V-shaped channels of the SFC and further downstream to the  
43 ICP-MS. Downstream of the electrochemical cell and prior to introduction into the ICP-MS the electrolyte  
44 was mixed with an internal standard using a Y-connector (mixing ratio 1:1). As internal standards for  
45  
46  
47  
48  
49  
50  
51  
52  
53  
54  
55  
56  
57  
58  
59  
60

1  
2  
3 detection of  $^{55}\text{Ti}$  and  $^{193}\text{Ir}$  isotopes, the isotopes of  $^{50}\text{Sc}$  or  $^{187}\text{Re}$  were used, respectively. The concentration  
4 of the internal standards in the solution was  $10\ \mu\text{gL}^{-1}$ . Calibration of the ICP-MS was performed on each  
5 experiment day prior to electrochemical measurements. The potentiostat (Gamry Reference 600, USA),  
6 electrolyte and gas flows as well as SFC components were automatically controlled using a homemade  
7 LabVIEW software. This enabled screening of the general behaviour of different locations on the material  
8 library under identical electrochemical protocols for direct comparison. Before the OER investigation the  
9 working electrode was always polarized at  $E=1.20\ \text{V}_{\text{RHE}}$  during 2 min for initial stabilization. Afterwards,  
10 the potential was swept from  $E=1.20\ \text{V}_{\text{RHE}}$  to a value corresponding to a current density of  $j=5\text{mAcm}^{-2}$   
11 with the scan rate of  $10\ \text{mV s}^{-1}$ . At least three measurements were done for each spot of the same  
12 composition to ensure the reproducibility of the results.  
13  
14  
15

16  
17 After this initial screening the long-term stability the most promising compositions that were synthesized  
18 as individual samples were tested in an H-cell with divided anodic and cathodic compartments. In a cell  
19 with such configuration the anodic and cathodic compartments were separated by a fine glass frit (Pine  
20 Research Instrumentation, USA). The volume of electrolyte in both compartments was adjusted to 10 mL  
21 and was kept constant during the measurements. A Pt foil placed in the cathodic compartment served as  
22 counter electrode. A saturated Ag/AgCl in the anodic compartment was used as a reference electrode.  
23  
24

25 The atom probe tomography (APT) experiments were conducted on a CAMECA LEAP 5000 XR instrument  
26 under laser pulsing mode at a specimen temperature of 60 K, with a target evaporation rate of 5 ions per  
27 1000 pulses, a pulsing rate of 125 kHz, laser pulse energy of 60 pJ. The APT specimens were prepared by  
28 a site-specific lift-out procedure using a FEI Helios G4 CX focused ion beam (FIB)/scanning electron  
29 microscope. A 200-nm thick protective Cr-layer was coated on top of the sputtered thin film by electron-  
30 beam deposition in order to protect the surface layers from FIB damage. The APT data were reconstructed  
31 and analysed using the commercial IVAS 3.8.4™ software.  
32  
33  
34

## 35 36 37 Results

38  
39 Characterization of Ir-TiO<sub>x</sub> libraries by X-ray photoelectron spectrometry.

40  
41 To ensure composition of the material library, XPS scans were recorded on as-deposited and thermally  
42 oxidized Ir-Ti composition gradient thin films. The atomic ratios between Ir and Ti remain the same after  
43 annealing at 350 °C for 4 h in air, which confirms an absence of significant segregation and diffusion of  
44 any of the elements within a thin surface layer during thermal treatment under these conditions. In all  
45 cases, iridium, titanium, oxygen and carbon were found on the surface. The spectra of Ir 4f, Ti 2p and O  
46 1s recorded on the thermally oxidized gradient sample containing 20, 40, 60 and 70 at.% of Ir are shown  
47 in Fig. 1. For all samples, the Ir 4f peak is observed at ca. 60.9 eV, indicating metallic state [35-38]. The  
48 symmetry of Ir 4f peak was observed to be independent of the Ir-Ti ratio, suggesting that the main line in  
49 Ir 4f level originates only from metallic Ir, or the amount of oxide species is below the detection limit.  
50 Regardless of the content of Ir in the samples its oxidation state remains constant. In the whole  
51 compositional range Ti 2p spectra have two resolved components. First, at lower binding energies (ca.  
52 454.6 eV) one that corresponds to metallic Ti, while the second at higher binding energies can be assigned  
53  
54  
55  
56  
57  
58  
59  
60

to Ti in oxides (ca 458.9 eV) [39]. The position of the peak corresponding to  $Ti^{0}$  is found to be independent of Ti content in the films, while its contribution decreases with lower Ti concentration. The peak corresponding to Ti oxides shifts from 458.9 eV ( $TiO_2$ ) to 458.4 eV as the content of Ir in the films increases from 20 to 70 at.%, most likely related to a decrease in oxygen stoichiometry of Ti oxides in Ir-enriched films. The O 1s spectra presented in Fig. 1c exhibit presence of two resolved components corresponding to O in the oxide lattice (at lower binding energies) and O from OH groups and water molecules on the electrode surface (at higher binding energies). With increasing content of Ir in the films the O 1s peak shifts from 530.4 eV to 529.8 eV. The contribution of OH and  $H_2O$  is also increasing. The observed variation can originate from the difference in the oxygen affinity for Ir and Ti. After the application of the electrochemical protocol no change in spectra of these elements was observed (Figure S4), which indirectly suggests high stability of these materials.

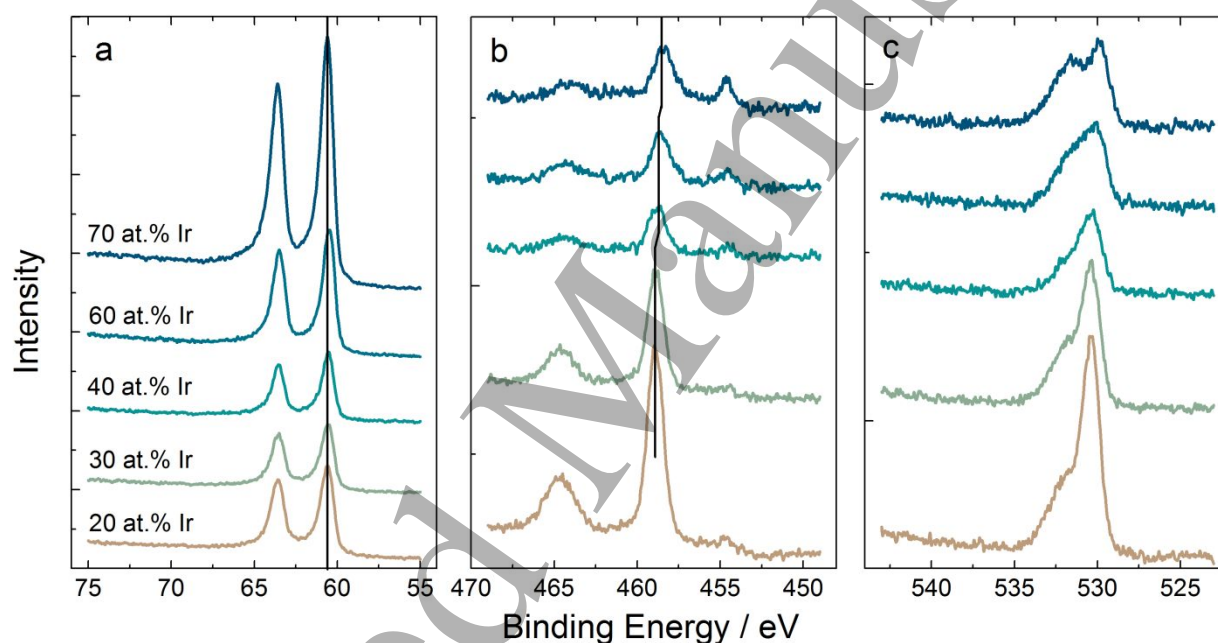
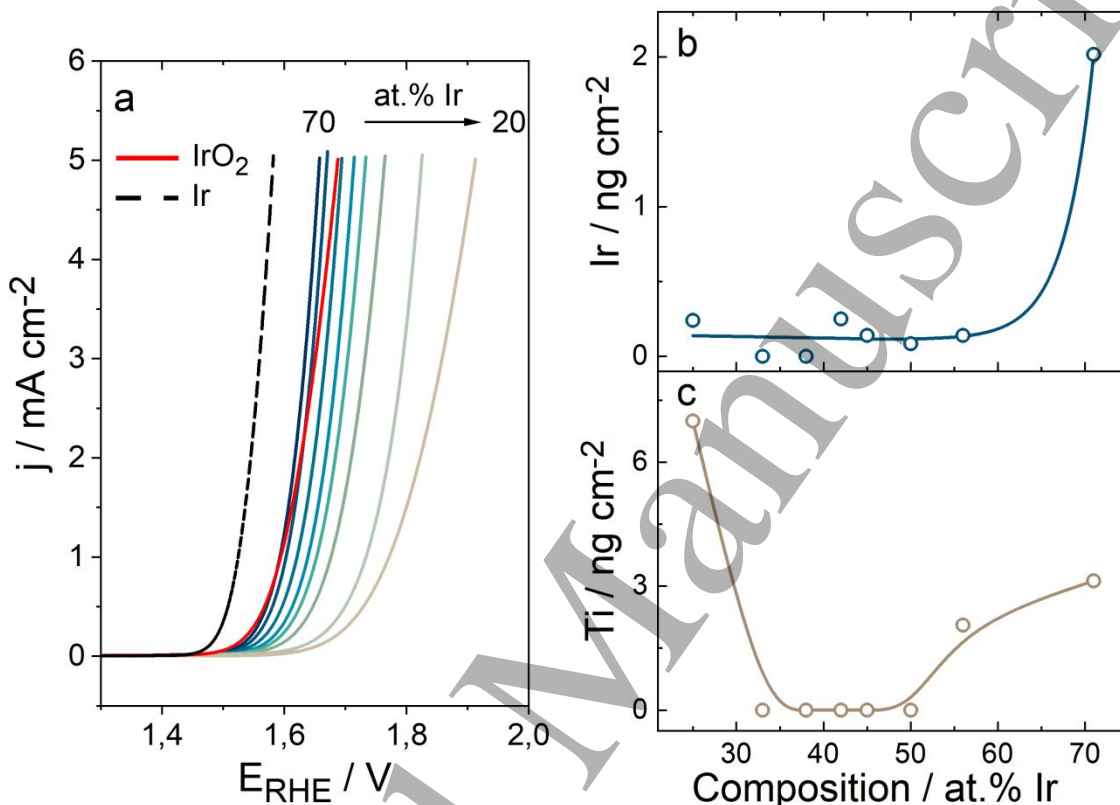


Figure 1. The XPS spectra of the Ir 4f (a), Ti 2p (b) and O 1s (c) levels for measurement areas with different Ir contents on thermally oxidized Ir- $TiO_x$  material library. The binding energies of Ir  $4f_{7/2}$  and Ti  $2p_{3/2}$  peaks are shown in black lines in (a) and (b), respectively.

Screening of Ir- $TiO_x$  material library for desired electrocatalytic properties.

Figure 2a shows anodic polarization curves recorded on the Ir- $TiO_x$  material library. For straightforward comparison with other materials examined by SFC-ICP-MS in the past, the value of potential at a current density of  $5 \text{ mA cm}^{-2}$  is chosen as a criterion of reactivity of these catalysts. In addition, the polarization curves for thermally prepared  $IrO_2$  and metallic Ir are presented for benchmarking. The benchmark Ir electrode was synthesized using magnetron sputtering under conditions similar to those for Ir-Ti mixtures, while  $IrO_2$  was prepared by annealing of such film in air at 600 C during 5 h to ensure formation of rutile phase [13]. Note, that in line with literature data [31] materials containing less than 20 at.% of Ir have poor conductivity and are not considered here. All of the investigated Ir- $TiO_x$  mixtures show lower

1  
2  
3 reactivity than metallic Ir, yet the materials with an Ir content of more than 50 at.% exhibit reactivity  
4 comparable to thermally grown IrO<sub>2</sub>. With decreasing Ir content in the material library, the potential at 5  
5 mA cm<sup>-2</sup> shifts to higher anodic values, i.e. the activity of the catalysts for the OER decreases.  
6  
7  
8  
9



36  
37 Figure 2. Summarized results on the activity-stability behaviour of Ir–TiO<sub>x</sub> material library. (a) Quasi  
38 steady-state anodic polarization curves for different Ir/Ti ratio of the material library in 0.1 M HClO<sub>4</sub>  
39 solution with a scan rate 10 mV s<sup>-1</sup>. (b) Simultaneously measured amounts of dissolved Ir and (c) Ti. As the  
40 benchmarks, polarization curves obtained on sputtered metallic Ir and IrO<sub>2</sub> prepared by thermal oxidation  
41 of sputtered metallic film are shown by dashed black and red curves, respectively.  
42

43  
44 The dissolution of Ir and Ti is measured simultaneously with the anodic potential sweep (LSV). Figures 2b  
45 and 2c summarize the integrated amounts of dissolved Ir and Ti during one LSV as a function of electrode  
46 composition. One can see that the rate of Ir dissolution in this short experiment remains negligible as long  
47 as its fraction in the electrode does not exceed 60 at.%. The loss of Ir from a sample containing 70 at.% of  
48 Ir was about 2 ng cm<sup>-2</sup>. For comparison, under the same electrochemical conditions about 0.2 ng cm<sup>-2</sup> of  
49 Ir is dissolved from thermally prepared IrO<sub>2</sub>, while a metallic electrode loses about 10 ng cm<sup>-2</sup> of Ir (see  
50 dissolution profiles in Figure S5). The dissolution of Ti is below the detection limit in the range of 30–50  
51 at.% of Ir, while it increases both at lower and higher Ir compositions. During the anodic potential sweep  
52 more than 7 ng cm<sup>-2</sup> Ti is removed from the electrodes containing less than 20 at.% of Ir, while at high Ir  
53 contents around 3 ng cm<sup>-2</sup> of Ti is lost. Considering that materials containing between 30 and 50 at.% of  
54  
55  
56  
57  
58  
59  
60

1  
2  
3 Ir show the best electrocatalytic performance, we further investigate the performance under long-term  
4 polarization of a representative sample within this composition range. Moreover, as the nonlinearity of  
5 the dissolution behaviour in this compositional range cannot be explained based on the XPS data only, the  
6 atomic scale structure of the 50 at.% of Ir sample is also considered in more detail.  
7  
8

9 Atomic scale insights into the composition of Ir-TiO<sub>x</sub> with 50 at.% of Ir.  
10

11 The atomic scale structure of an Ir-TiO<sub>x</sub> electrode with 50 at.% of Ir was revealed by atom probe  
12 tomography (APT). APT provides information on the elemental distribution in three dimensions [40-42].  
13 Figures 3a and 3b show the side and top-down views of the 3D APT reconstruction of a catalyst film,  
14 respectively. The profiles in Figure c-e show the compositional variations in a near surface layer, bulk, and  
15 lateral surface. Based on the APT data the volume of the catalyst can be described as a composite alloy  
16 containing matrix with the nominal composition of 40 at.% of Ir decorated with Ti enriched regions. The  
17 content of Ti in such clusters ranges from 70 to 80 at.%. The average composition roughly corresponds to  
18 50 at.% of Ir, in line with EDX and XPS data. The composition profiles of the near surface region are shown  
19 in Fig. 3c and 3e. The data suggests that the thermal oxidation occurs in the near surface regions and only  
20 Ti-enriched clusters are prone to oxidize. The composition of the oxide clusters in the near surface region  
21 corresponds to 70 at% of Ti, 25 at% of O and 5 at% of Ir. The oxygen content tends to decrease with the  
22 depth. The composition of the metallic matrix in the top surface region increases to 50 at.% Ir as was also  
23 revealed by XPS (Figure 3c). Distribution of oxygen is inhomogeneous in all directions.  
24  
25  
26  
27  
28  
29  
30  
31  
32  
33  
34  
35  
36  
37  
38  
39  
40  
41  
42  
43  
44  
45  
46  
47  
48  
49  
50  
51  
52  
53  
54  
55  
56  
57  
58  
59  
60



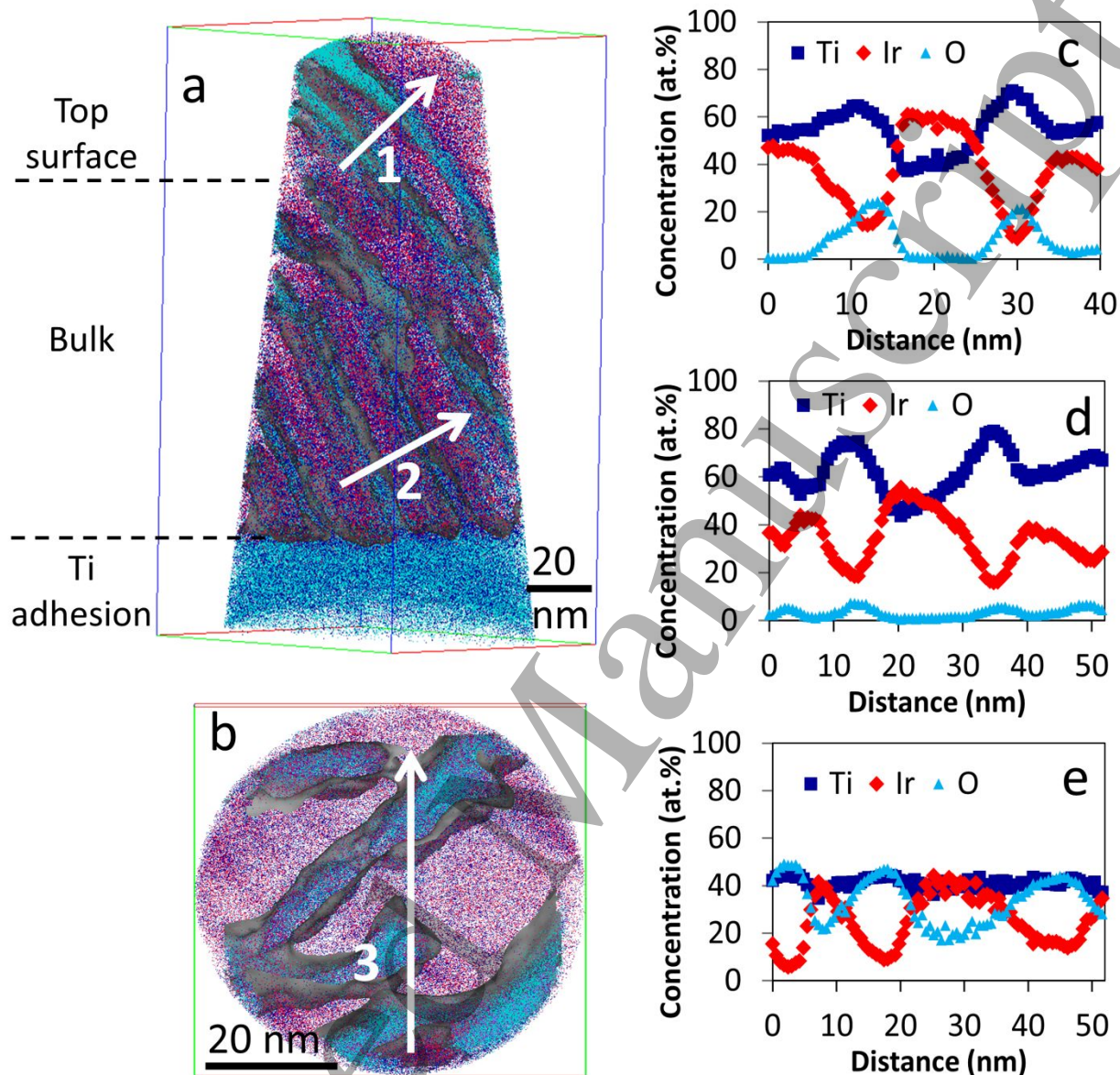


Figure 3. APT data on Ir-TiO<sub>x</sub> containing 50 at.% of Ir. (a) Side view of APT reconstruction of the as-deposited sample. (b) Top-down view of APT reconstruction. (c), (d) and (e), One-dimensional composition profiles from the regions along the arrows labelled 1, 2 and 3 in (a) and (b). The grey areas show Ti-enriched regions, with the content of Ti in the range of 50-80 at.%. The Cr protective layer is not shown in the reconstruction.

Long-term performance of the Ir-TiO<sub>x</sub> anode containing 50 at.% of Ir.

The SFC-ICP-MS measurements for gas evolving reactions are typically limited due to possible blocking of the working electrode by bubble formation over time, which is why they can only provide a first information on the initial dissolution rates. In order to examine the long-term stability of anode materials, galvanostatic measurements are performed in an H-cell with divided anodic and cathodic compartments.

In these experiments samples of the electrolyte are taken periodically from both compartments for analysis of metal content using off-line ICP-MS. During the entire experiment no Ir nor Ti was detected in the cathodic compartment. In the anodic compartment only after 120 min significant metal dissolution could be found (Figure 4). The Ti concentration remains constant below  $1 \text{ ng cm}^{-2}$  after ca. 120 min, while it takes about 200 min for the Ir concentration to stabilize at around  $8 \text{ ng cm}^{-2}$ . Note that this equilibrium might be special for the given H-cell and the volume of electrolyte, and surely differs from the behaviour of flow reactors where due to the constant purging such an equilibrium might not be reached. For straightforward comparison of evolution of the electrocatalytic activity of the electrode the quasi steady state polarization curve was taken after the H-cell experiments (curve 2 in Fig. S6). In these conditions to achieve current density of  $5 \text{ mA cm}^{-2}$  additional 25 mV are required, which indicates slight drop of activity.

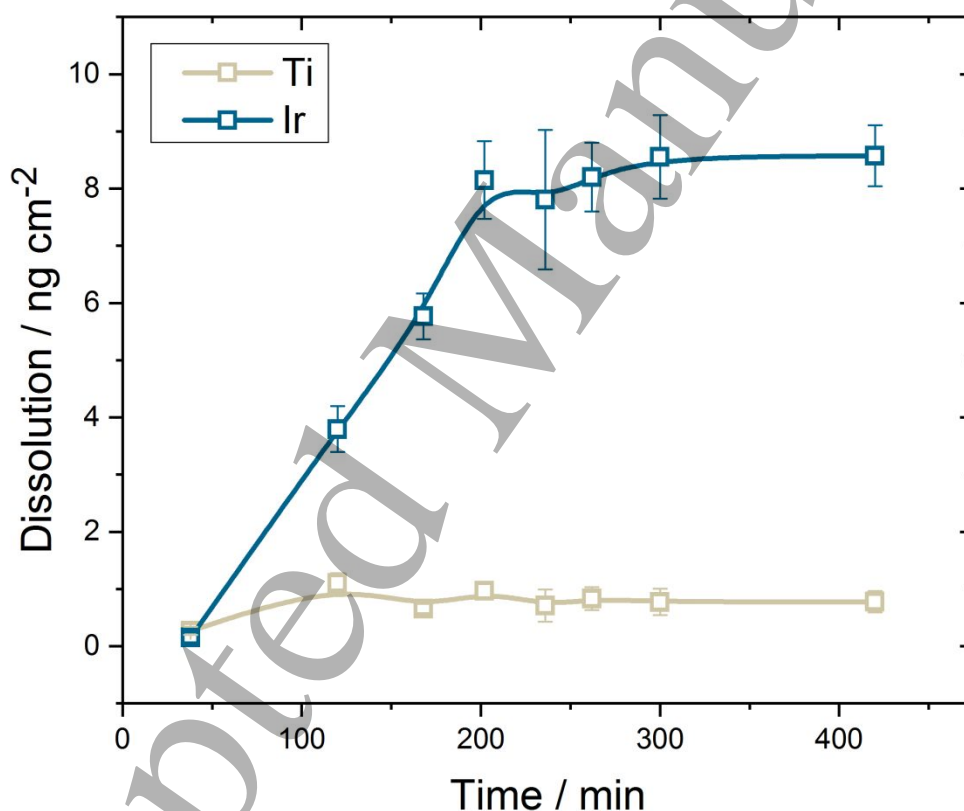


Figure 4. Dependence of the amount of dissolved Ir and Ti from an Ir-TiO<sub>x</sub> anode containing 50 at.% Ir on electrolysis duration. The anodic polarization was performed in an H-cell with divided anodic and cathodic compartment at  $1 \text{ mA cm}^{-2}$  in  $0.1 \text{ M HClO}_4$ .

## Discussion

Catalyst materials prepared by dispersing the noble metals in a more stable nonprecious matrix have been intensively investigated. Among others, TiO<sub>2</sub>-containing mixtures were successfully employed in

1  
2  
3 dimensionally stable anodes for chlorine evolution [10, 43]. For OER related applications the main  
4 research efforts were focused on reduction of the amount of the noble metal in the electrode without a  
5 significant decrease in electronic conductivity and reactivity [9]. As was shown in literature [31], the  
6 reduction of the Ir content in Ir/TiO<sub>x</sub> results in drastic changes in electrical conductivity and the  
7 respective OER performance as a catalyst. Anodes containing various mixtures of Ti, Ir and Sn were shown  
8 to have improved stability, though the activity was lower than metallic Ir and also what thermally  
9 annealed IrO<sub>2</sub> could provide [44]. Here, the screening of the Ir-TiO<sub>x</sub> materials library (Figure 2) shows that  
10 the activity of such mixtures can be comparable to IrO<sub>2</sub>. The XPS data in Figure 1 confirms the initial  
11 metallic state of Ir in the whole compositional range that leads to the high reactivity, when the sample  
12 only experiences a moderate thermal treatment of short duration. Apparently, the oxidation of Ir is  
13 hindered during short-term treatment in air at rather mild temperatures. It was previously reported that  
14 the heat-treatment at temperatures below 400 C is not sufficient to form rutile IrO<sub>2</sub> [45-47]. Considering  
15 the high affinity of Ti for oxygen, its presence in the electrodes makes oxidation of Ir relatively even more  
16 unfavorable. The oxidation of Ti is also incomplete independent of the composition, which could be  
17 explained by either the low partial pressure of oxygen in air, as well as the low temperature and duration  
18 of the annealing treatment or limited diffusion of oxygen into the film. This results in sufficiently high  
19 conductivity. In line with previous reports [48], the reactivity decreases with increasing content of Ti in  
20 the electrode (Figure 2a). This can be explained by both the decrease in the number of electrochemically  
21 active sites provided exclusively by Ir and the increasing contribution of less conductive oxides of Ti (Figure  
22 2b). The observed trend supports previously published statements on the overall deterioration in OER  
23 activity at high Ti contents in binary noble metals-based mixed oxides, including those containing Ir [31,  
24 48, 49].

25  
26  
27  
28  
29  
30  
31  
32 Stability data demonstrates the increase in Ir dissolution with its increasing content in the electrode (Fig.  
33 2b). A higher Ir loading on the surface of the electrode results in an increased number of active sites  
34 available for the OER and improved activity. Considering our previous reports suggesting that Ir  
35 dissolution is triggered by the OER itself [16, 17, 50], the amount of dissolved Ir should increase with  
36 increasing activity. A similar dissolution behaviour was previously reported for Ir-Ru mixed oxides [51].  
37 However, in contrast to the Ir-Ru system where both components show increased dissolution with their  
38 increasing content, the dependence of Ti dissolution from Ir-TiO<sub>x</sub> anodes on the electrode composition is  
39 more complex (Figure 2c). In particular, the Ti dissolution rate increases at both high and low loadings of  
40 Ti in the films, while at the mid-composition range the dissolution is below the detection limit in SFC-ICP-  
41 MS experiments. Apparently, the dissolution of Ti results from the metallic phase present in the films, as  
42 shown by XPS data in Figure 1b. Under OER conditions this metallic phase converts into an oxide, which is  
43 accompanied by dissolution, as was reported previously [41]. According to the XPS data in Figure 1c the  
44 content of metallic Ti phase increases for materials with high Ir loadings and so does the dissolution. In  
45 contrast, a high dissolution rate of Ti at low Ir contents can be explained by the significant drop in the  
46 activity, leading to more positive anodic potential at the current density of 5 mA cm<sup>-2</sup>. Interestingly,  
47 mixtures containing ca 30 – 50 at.% of Ir exhibit an extraordinary immunity towards dissolution of both  
48 components, which results from the formation of Ti-enriched oxide regions with superior stability as  
49 revealed by APT (Figure 3). The overall non-linear activity-stability relationship in such materials originates  
50 from the coexistence of highly reactive metallic Ir and a stable phase of titanium oxides. The catalytic  
51  
52  
53  
54  
55  
56  
57  
58  
59  
60

properties of materials containing a Ti oxide phase tend to suffer from their semiconducting or even insulating nature. However, for the 50% sample investigated in more detail here the APT data (Figure 3) reveals that the titanium oxide phase contains with at least 5 at.% of Ir, which boosts the conductivity of the catalytic layer.

In order to compare the stability behaviour of Ir-TiO<sub>x</sub> to other thin film catalysts we estimated their stability numbers (S-number) in conditions of quasi-steady state anodic polarization at 1 mA cm<sup>-2</sup> based on the data in Figure 4. The S-number is a universal metric independent of the surface area and catalyst loading (in case of nanoparticles), and corresponds to the number of oxygen molecules evolved versus the amount of dissolved catalytically active atoms (herein Ir) [50]. Considering the summarized data shown in Table 1, all OER catalysts exhibit S-numbers comparable to that of amorphous IrO<sub>x</sub>. Although the Ir-Ru mixed oxide also shows a relatively high S-number for Ir, it should be considered that in this case the OER occurs mainly on Ru active sites, resulting in intense Ru corrosion, while Ir contributes to the reaction to a lesser extent. The Ir-TiO<sub>x</sub> anode exhibits high stability with an S-number comparable to that reported for thermally grown IrO<sub>2</sub>, exceeding previously reported performance of IrO<sub>2</sub>@TiO<sub>2</sub> nanoparticles [26]. Even though a direct comparison of thin film materials with nanoparticles is rather complicated, the observed difference in durability estimation suggests that formation of the mixed oxide phase of Ir and Ti is crucial for the stability of the catalyst and requires further investigation and optimization.

Table 1. The S-number calculated for different Ir-containing catalysts.

Anode material	S-number*	Conditions	Reference
Ir <sub>0.5</sub> Ti <sub>0.5</sub> O <sub>x</sub>	1.5·10 <sup>6</sup>	0.1 M HClO <sub>4</sub> ; steady-state, 1 mA cm <sup>-2</sup>	This work
Ir <sub>0.7</sub> Sn <sub>0.3</sub> O <sub>x</sub>	1.6·10 <sup>5</sup>	0.1 M HClO <sub>4</sub> ; steady-state, 1 mA cm <sup>-2</sup>	[23, 52]
	5·10 <sup>4</sup>	0.1 M HClO <sub>4</sub> ; 5 min, 1 mA cm <sup>-2</sup>	
Ir <sub>0.7</sub> Ru <sub>0.3</sub> O <sub>2</sub> **	1.0·10 <sup>6</sup> (Ir) *** 1.0·10 <sup>5</sup> (Ru)	0.1 M HClO <sub>4</sub> ; 1 min, 1 mA cm <sup>-2</sup>	[51, 52]
IrO <sub>2</sub>	9.2·10 <sup>5</sup>	0.1 M HClO <sub>4</sub> ; 10 min, 1 mA cm <sup>-2</sup>	[50]
IrO <sub>x</sub> -amorphous	5.0·10 <sup>4</sup>	0.1 M HClO <sub>4</sub> ; 5 min, 1 mA cm <sup>-2</sup>	[50]
Ir metal	1.0·10 <sup>5</sup>	0.1 M HClO <sub>4</sub> ; 5 min, 1 mA cm <sup>-2</sup>	[50]
SrIrO <sub>3</sub> , thin film	8.0·10 <sup>4</sup>	0.1 M HClO <sub>4</sub> ; 10 min, 1 mA cm <sup>-2</sup>	[50]
IrO <sub>2</sub> @TiO <sub>2</sub> NPs	1.0·10 <sup>4</sup>	0.1 M HClO <sub>4</sub> ; 5 min, 100 mA mg <sup>-1</sup>	[26]

\*For alloys and mixed oxides, the S-number should be considered for all elements reactive towards the OER

\*\*Here, dissolution of both Ir and Ru was normalized by the total amount of formed oxygen molecules, since the number of oxygen molecules evolved on each type of active sites remains unknown

\*\*\*In Ir<sub>0.7</sub>Ru<sub>0.3</sub>O<sub>2</sub> anode the OER mainly takes place on the more reactive Ru active sites, which explains the high stability number for Ir. However, dissolution of both elements should be considered for the overall stability.

Although long-term durability of Ir-Ti mixtures has still to be proven, the addition of Ti oxide to Ir seems to be a promising way to achieve the balance between activity and stability and decrease the Ir loading. Important to note is, however, that the stability of Ir in such systems can suffer from conductivity issues leading to potential shifts and further dissolution. Thorough analysis of the electronic properties of Ir-Ti mixtures has to be considered for the design of superior catalysts. A comprehensive study of the relationship between electronic properties and activity/stability for such mixed oxide anodes in acidic media will be a topic of a future work.

## Conclusions

1  
2  
3 Stability and activity towards the OER of a model Ir–Ti mixed oxide materials library over a wide  
4 composition range were examined using the SFC-ICP-MS set-up. The results concerning the dissolution of  
5 Ir and Ti show that independent of the Ir content in the electrode, the rate of its dissolution is observed  
6 to be lower than that of thermally prepared IrO<sub>2</sub>, while catalysts containing at least 50 at.% of Ir exhibit  
7 relatively high activity. This beneficial balance between activity and stability originates from the atomic-  
8 scale structure of this catalyst in which metallic Ir, providing high activity, coexists with Ti-enriched oxide  
9 phases, which ensure stability towards dissolution. Overall, our data show that Ir-Ti mixtures can be  
10 promising OER catalysts with both high activity and stability against dissolution.  
11  
12  
13

#### 14 Acknowledgments

15  
16 O.K. acknowledges financial support from the Helmholtz Networking and Initiative Fund. The use of APT  
17 and FIB of ZGH, RUB are acknowledged.  
18  
19

#### 20 References

- 21  
22 [1] F. Barbir, PEM electrolysis for production of hydrogen from renewable energy sources, *Solar Energy*,  
23 78 (2005) 661-669.  
24 [2] J. Rossmesl, Z.W. Qu, H. Zhu, G.J. Kroes, J.K. Nørskov, Electrolysis of water on oxide surfaces, *Journal*  
25 *of Electroanalytical Chemistry*, 607 (2007) 83-89.  
26 [3] S. Trasatti, Electrochemistry and environment: The role of electrocatalysis, *International Journal of*  
27 *Hydrogen Energy*, 20 (1995) 835-844.  
28 [4] M. Carmo, D.L. Fritz, J. Mergel, D. Stolten, A comprehensive review on PEM water electrolysis,  
29 *International Journal of Hydrogen Energy*, 38 (2013) 4901-4934.  
30 [5] N. Danilovic, K.E. Ayers, C. Capuano, J.N. Renner, L. Wiles, M. Pertoso, (Plenary) Challenges in Going  
31 from Laboratory to Megawatt Scale PEM Electrolysis, *ECS Transactions*, 75 (2016) 395-402.  
32 [6] T. Binninger, R. Mohamed, K. Waltar, E. Fabbri, P. Levecque, R. Kotz, T.J. Schmidt, Thermodynamic  
33 explanation of the universal correlation between oxygen evolution activity and corrosion of oxide  
34 catalysts, *Scientific reports*, 5 (2015) 12167.  
35 [7] N. Danilovic, R. Subbaraman, K.-C. Chang, S.H. Chang, Y.J. Kang, J. Snyder, A.P. Paulikas, D. Strmcnik,  
36 Y.-T. Kim, D. Myers, V.R. Stamenkovic, N.M. Markovic, Activity–Stability Trends for the Oxygen Evolution  
37 Reaction on Monometallic Oxides in Acidic Environments, *The journal of physical chemistry letters*, 5  
38 (2014) 2474-2478.  
39 [8] N. Hodnik, P. Jovanovič, A. Pavlišič, B. Jozinovič, M. Zorko, M. Bele, V.S. Šelih, M. Šala, S. Hočevar, M.  
40 Gaberšček, New Insights into Corrosion of Ruthenium and Ruthenium Oxide Nanoparticles in Acidic  
41 Media, *The Journal of Physical Chemistry C*, 119 (2015) 10140-10147.  
42 [9] S. Trasatti, Electrocatalysis in the anodic evolution of oxygen and chlorine, *Electrochimica Acta*, 29  
43 (1984) 1503-1512.  
44 [10] S. Trasatti, Electrocatalysis: understanding the success of DSA®, *Electrochimica Acta*, 45 (2000)  
45 2377-2385.  
46 [11] M. Schalenbach, G. Tjarks, M. Carmo, W. Lueke, M. Mueller, D. Stolten, Acidic or Alkaline? Towards  
47 a New Perspective on the Efficiency of Water Electrolysis, *Journal of The Electrochemical Society*, 163  
48 (2016) F3197-F3208.  
49 [12] S. Siracusano, N. Hodnik, P. Jovanovic, F. Ruiz-Zepeda, M. Šala, V. Baglio, A.S. Aricò, New insights  
50 into the stability of a high performance nanostructured catalyst for sustainable water electrolysis, *Nano*  
51 *Energy*, 40 (2017) 618-632.  
52  
53  
54  
55  
56  
57  
58  
59  
60

- [13] S. Cherevko, S. Geiger, O. Kasian, N. Kulyk, J.-P. Grote, A. Savan, B.R. Shrestha, S. Merzlikin, B. Breitbach, A. Ludwig, K.J.J. Mayrhofer, Oxygen and hydrogen evolution reactions on Ru, RuO<sub>2</sub>, Ir, and IrO<sub>2</sub> thin film electrodes in acidic and alkaline electrolytes: A comparative study on activity and stability, *Catalysis Today*, 262 (2016) 170-180.
- [14] S. Cherevko, A.R. Zeradjanin, A.A. Topalov, N. Kulyk, I. Katsounaros, K.J.J. Mayrhofer, Dissolution of Noble Metals during Oxygen Evolution in Acidic Media, *ChemCatChem*, 6 (2014) 2219-2223.
- [15] P. Jovanovič, N. Hodnik, F. Ruiz-Zepeda, I. Arcon, B. Jozinovič, M. Zorko, M. Bele, M. Šala, V.S. Šelih, S.B. Hocevar, M. Gaberscek, Electrochemical Dissolution of Iridium and Iridium Oxide Particles in Acidic Media: Transmission Electron Microscopy, Electrochemical Flow Cell Coupled to Inductively Coupled Plasma Mass Spectrometry and X-ray Absorption Spectroscopy Study, *Journal of the American Chemical Society*, (2017).
- [16] O. Kasian, J.-P. Grote, S. Geiger, S. Cherevko, K.J.J. Mayrhofer, The common Intermediates of Oxygen Evolution and Dissolution Reactions during Water Electrolysis on Iridium, *Angewandte Chemie International Edition*, 57 (2018).
- [17] O. Kasian, S. Geiger, T. Li, J.-P. Grote, K. Schweinar, S. Zhang, C. Scheu, D. Raabe, S. Cherevko, B. Gault, K.J.J. Mayrhofer, Degradation of iridium oxides via oxygen evolution from the lattice: correlating atomic scale structure with reaction mechanisms, *Energy & Environmental Science*, 12 (2019) 3548-3555.
- [18] S. Choe, B.-S. Lee, M.K. Cho, H.-J. Kim, D. Henkensmeier, S.J. Yoo, J.Y. Kim, S.Y. Lee, H.S. Park, J.H. Jang, Electrodeposited IrO<sub>2</sub>/Ti electrodes as durable and cost-effective anodes in high-temperature polymer-membrane-electrolyte water electrolyzers, *Applied Catalysis B: Environmental*, 226 (2018) 289-294.
- [19] Y. Kamegaya, K. Sasaki, M. Oguri, T. Asaki, H. Kobayashi, T. Mitamura, Improved durability of iridium oxide coated titanium anode with interlayers for oxygen evolution at high current densities, *Electrochimica Acta*, 40 (1995) 889-895.
- [20] G. Li, K. Li, L. Yang, J. Chang, R. Ma, Z. Wu, J. Ge, C. Liu, W. Xing, Boosted Performance of Ir Species by Employing TiN as the Support toward Oxygen Evolution Reaction, *ACS Applied Materials & Interfaces*, 10 (2018) 38117-38124.
- [21] M. Bernt, H.A. Gasteiger, Influence of Ionomer Content in IrO<sub>2</sub>/TiO<sub>2</sub> Electrodes on PEM Water Electrolyzer Performance, *Journal of The Electrochemical Society*, 163 (2016) F3179-F3189.
- [22] A. Lončar, L. Moriau, K. Stojanovski, F. Ruiz-Zepeda, P. Jovanovic, M. Bele, M. Gaberscek, N. Hodnik, Ir/TiO<sub>n</sub>/C high-performance oxygen evolution reaction nanocomposite electrocatalysts in acidic media: synthesis, characterization and electrochemical benchmarking protocol, *Journal of Physics: Energy*, 2 (2020).
- [23] O. Kasian, S. Geiger, M. Schalenbach, A.M. Mingers, A. Savan, A. Ludwig, S. Cherevko, K.J.J. Mayrhofer, Using Instability of a Non-stoichiometric Mixed Oxide Oxygen Evolution Catalyst As a Tool to Improve Its Electrocatalytic Performance, *Electrocatalysis*, 9 (2018) 139-145.
- [24] G. Li, H. Yu, D. Yang, J. Chi, X. Wang, S. Sun, Z. Shao, B. Yi, Iridium-Tin oxide solid-solution nanocatalysts with enhanced activity and stability for oxygen evolution, *Journal of Power Sources*, 325 (2016) 15-24.
- [25] G. Liu, J. Xu, Y. Wang, X. Wang, An oxygen evolution catalyst on an antimony doped tin oxide nanowire structured support for proton exchange membrane liquid water electrolysis, *Journal of Materials Chemistry A*, 3 (2015) 20791-20800.
- [26] C.V. Pham, M. Bühler, J. Knöppel, M. Bierling, D. Seeberger, D. Escalera-López, K.J.J. Mayrhofer, S. Cherevko, S. Thiele, IrO<sub>2</sub> coated TiO<sub>2</sub> core-shell microparticles advance performance of low loading proton exchange membrane water electrolyzers, *Applied Catalysis B: Environmental*, 269 (2020) 118762.
- [27] P. Mazúr, J. Polonský, M. Paidar, K. Bouzek, Non-conductive TiO<sub>2</sub> as the anode catalyst support for PEM water electrolysis, *International Journal of Hydrogen Energy*, 37 (2012) 12081-12088.

- [28] H. Lv, G. Zhang, C. Hao, C. Mi, W. Zhou, D. Yang, B. Li, C. Zhang, Activity of IrO<sub>2</sub> supported on tantalum-doped TiO<sub>2</sub> electrocatalyst for solid polymer electrolyte water electrolyzer, *RSC Advances*, 7 (2017) 40427-40436.
- [29] H.-S. Oh, H.N. Nong, D. Teschner, T. Reier, A. Bergmann, M. Gliech, J. Ferreira de Araújo, E. Willinger, R. Schloegl, P. Strasser, Electrochemical catalyst-support effects and their stabilizing role for IrO<sub>x</sub> nanoparticle catalysts during the oxygen evolution reaction (OER), *Journal of the American Chemical Society*, (2016).
- [30] V.A. Saveleva, L. Wang, O. Kasian, M. Batuk, J. Hadermann, J.J. Gallet, F. Bournel, N. Alonso-Vante, G. Ozouf, C. Beauger, K.J.J. Mayrhofer, S. Cherevko, A.S. Gago, K.A. Friedrich, S. Zafeiratos, E.R. Savinova, Insight into the Mechanisms of High Activity and Stability of Iridium Supported on Antimony-Doped Tin Oxide Aerogel for Anodes of Proton Exchange Membrane Water Electrolyzers, *ACS Catalysis*, 10 (2020) 2508-2516.
- [31] D. Bernsmeier, M. Bernicke, R. Schmack, R. Sachse, B. Paul, A. Bergmann, P. Strasser, E. Ortel, R. Kraehnert, Oxygen Evolution Catalysts Based on Ir–Ti Mixed Oxides with Templated Mesopore Structure: Impact of Ir on Activity and Conductivity, *ChemSusChem*, 11 (2018) 2367-2374.
- [32] E. Oakton, D. Lebedev, M. Povia, D.F. Abbott, E. Fabbri, A. Fedorov, M. Nachttegaal, C. Copéret, T.J. Schmidt, IrO<sub>2</sub>-TiO<sub>2</sub>: A High-Surface-Area, Active, and Stable Electrocatalyst for the Oxygen Evolution Reaction, *ACS Catalysis*, 7 (2017) 2346-2352.
- [33] A.K. Schuppert, A.A. Topalov, A. Savan, A. Ludwig, K.J.J. Mayrhofer, Composition-Dependent Oxygen Reduction Activity and Stability of Pt-Cu Thin Films, *ChemElectroChem*, 1 (2014) 358-361.
- [34] A.A. Topalov, I. Katsounaros, M. Auinger, S. Cherevko, J.C. Meier, S.O. Klemm, K.J.J. Mayrhofer, Dissolution of Platinum: Limits for the Deployment of Electrochemical Energy Conversion?, *Angewandte Chemie International Edition*, 51 (2012) 12613-12615.
- [35] J. Augustynski, M. Koudelka, J. Sanchez, B.E. Conway, ESCA study of the state of iridium and oxygen in electrochemically and thermally formed iridium oxide films, *Journal of Electroanalytical Chemistry and Interfacial Electrochemistry*, 160 (1984) 233-248.
- [36] C. Massué, V. Pfeifer, M. van Gastel, J. Noack, G. Algara-Siller, S. Cap, R. Schlögl, Reactive Electrophilic OI– Species Evidenced in High-Performance Iridium Oxohydroxide Water Oxidation Electrocatalysts, *ChemSusChem*, 10 (2017) 4786-4798.
- [37] V. Pfeifer, T.E. Jones, J.J. Velasco Vélez, C. Massué, R. Arrigo, D. Teschner, F. Girgsdies, M. Scherzer, M.T. Greiner, J. Allan, M. Hashagen, G. Weinberg, S. Piccinin, M. Hävecker, A. Knop-Gericke, R. Schlögl, The electronic structure of iridium and its oxides, *Surface and Interface Analysis*, 48 (2016) 261-273.
- [38] V. Pfeifer, T.E. Jones, J.J. Velasco Velez, C. Massue, M.T. Greiner, R. Arrigo, D. Teschner, F. Girgsdies, M. Scherzer, J. Allan, M. Hashagen, G. Weinberg, S. Piccinin, M. Havecker, A. Knop-Gericke, R. Schlogl, The electronic structure of iridium oxide electrodes active in water splitting, *Physical Chemistry Chemical Physics*, 18 (2016) 2292-2296.
- [39] L.A. da Silva, V.A. Alves, S.C. de Castro, J.F.C. Boodts, XPS study of the state of iridium, platinum, titanium and oxygen in thermally formed IrO<sub>2</sub> +TiO<sub>2</sub> +PtO<sub>x</sub> films, *Colloids and Surfaces A: Physicochemical and Engineering Aspects*, 170 (2000) 119-126.
- [40] J. Lim, S.-H. Kim, R. Aymerich Armengol, O. Kasian, P.-P. Choi, L.T. Stephenson, B. Gault, C. Scheu, Atomic-Scale Mapping of Impurities in Partially Reduced Hollow TiO<sub>2</sub> Nanowires, *Angewandte Chemie International Edition*, 59 (2020) 5651-5655.
- [41] K. Schweinar, B. Gault, I. Mouton, O. Kasian, Lattice Oxygen Exchange in Rutile IrO<sub>2</sub> during the Oxygen Evolution Reaction, *The journal of physical chemistry letters*, 11 (2020) 5008-5014.
- [42] K. Schweinar, R.L. Nicholls, C.R. Rajamathi, P. Zeller, M. Amati, L. Gregoratti, D. Raabe, M. Greiner, B. Gault, O. Kasian, Probing catalytic surfaces by correlative scanning photoemission electron microscopy and atom probe tomography, *Journal of Materials Chemistry A*, 8 (2020) 388-400.



- 1  
2  
3 [43] V.V. Gorodetskii, V.A. Neburchilov, V.I. Alyab'eva, <Titanium Anodes with an Active Coating Based  
4 on Iridium Oxides.pdf>, Russian Journal of Electrochemistry, 41 (2005) 1111–1117.  
5 [44] E. Antolini, Iridium As Catalyst and Cocatalyst for Oxygen Evolution/Reduction in Acidic Polymer  
6 Electrolyte Membrane Electrolyzers and Fuel Cells, ACS Catalysis, 4 (2014) 1426-1440.  
7 [45] S. Geiger, O. Kasian, B.R. Shrestha, A.M. Mingers, K.J.J. Mayrhofer, S. Cherevko, Activity and Stability  
8 of Electrochemically and Thermally Treated Iridium for the Oxygen Evolution Reaction, Journal of The  
9 Electrochemical Society, 163 (2016) F3132-F3138.  
10 [46] V.V. Gorodetskii, V.A. Neburchilov, Tantalum oxide effect on the surface structure and morphology  
11 of the IrO<sub>2</sub> and IrO<sub>2</sub> + RuO<sub>2</sub> + TiO<sub>2</sub> coatings and on the corrosion and electrochemical properties of  
12 anodes prepared from these, Russian Journal of Electrochemistry, 43 (2007) 223-228.  
13 [47] S. Cherevko, T. Reier, A.R. Zeradjanin, Z. Pawolek, P. Strasser, K.J.J. Mayrhofer, Stability of  
14 nanostructured iridium oxide electrocatalysts during oxygen evolution reaction in acidic environment,  
15 Electrochemistry Communications, 48 (2014) 81-85.  
16 [48] K. Endo, Y. Katayama, T. Miura, T. Kishi, Composition Dependence of the Oxygen-Evolution Reaction  
17 Rate on Ir x Ti<sub>1-x</sub> O<sub>2</sub> Mixed-Oxide Electrodes, Journal of Applied Electrochemistry - J APPL  
18 ELECTROCHEM, 32 (2002) 173-178.  
19 [49] O.I. Kasian, T.V. Luk'yanenko, A.B. Velichenko, Electrochemical properties of heat-treated platinumized  
20 titanium, Protection of Metals and Physical Chemistry of Surfaces, 49 (2013) 559-566.  
21 [50] S. Geiger, O. Kasian, M. Ledendecker, E. Pizzutilo, A.M. Mingers, W.T. Fu, O. Diaz-Morales, Z. Li, T.  
22 Oellers, L. Fruchter, A. Ludwig, K.J.J. Mayrhofer, M.T.M. Koper, S. Cherevko, The stability number as a  
23 metric for electrocatalyst stability benchmarking, Nature Catalysis, (2018).  
24 [51] O. Kasian, S. Geiger, P. Stock, G. Polymeros, B. Breitbach, A. Savan, A. Ludwig, S. Cherevko, K.J.J.  
25 Mayrhofer, On the Origin of the Improved Ruthenium Stability in RuO<sub>2</sub>–IrO<sub>2</sub> Mixed Oxides, Journal of  
26 The Electrochemical Society, 163 (2016) F3099-F3104.  
27 [52] O. Kasian, S. Geiger, K.J.J. Mayrhofer, S. Cherevko, Electrochemical On-line ICP-MS in  
28 Electrocatalysis Research, The Chemical Record, 19 (2019) 2130-2142.  
29  
30  
31  
32  
33  
34  
35  
36  
37  
38  
39  
40  
41  
42  
43  
44  
45  
46  
47  
48  
49  
50  
51  
52  
53  
54  
55  
56  
57  
58  
59  
60